

Design and Use of a Thermogelling Methylcellulose Nanoemulsion to Formulate Nanocrystalline Oral Dosage Forms

Liang-Hsun Chen and Patrick S. Doyle*

Oral drug products have become indispensable in modern medicine because of their exceptional patient compliance. However, poor bioavailability of ubiquitous low-water-soluble active pharmaceutical ingredients (APIs) and lack of efficient oral drug formulations remain as significant challenges. Nanocrystalline formulations are an attractive route to increase API solubility, but typically require abrasive mechanical milling and several processing steps to create an oral dosage form. Using the dual amphiphilic and thermoresponsive properties of methylcellulose (MC), a new thermogelling nanoemulsion and a facile thermal dripping method are developed for efficient formulation of composite particles with the MC matrix embedded with precisely controlled API nanocrystals. Moreover, a fast and tunable release performance is achieved with the combination of a fast-eroding MC matrix and fast-dissolving API nanocrystals. Using the versatile thermal processing approach, the thermogelling nanoemulsion is easily formulated into a wide variety of dosage forms (nanoparticle suspension, drug tablet, and oral thin film) in a manner that avoids nanomilling. Overall, the proposed thermogelling nanoemulsion platform not only broadens the applications of thermoresponsive nanoemulsions but also shows great promise for more efficient formulation of oral drug products with high quality and tunable fast release.

acceptance.^[2,3] However, conventional oral drug formulations typically require costly multistep manufacturing, and poor bioavailability of hydrophobic APIs still remains a persistent challenge in many formulations. It has been reported that 40% of marketed drugs and 90% of drug candidates in the pipeline are hydrophobic.^[4] Their poor water-solubility renders the drugs difficult to be absorbed in the gastrointestinal tract, greatly undermining their potency. Over the past decade, many attempts have been made to develop methods for producing API nanocrystals that possess improved solubility and bioavailability because of their significantly larger specific surface area compared to their bulk counterparts.^[5–7] However, incorporation of the methods into conventional formulation processes is susceptible to many problems. For example, suitable excipients have to be investigated through tedious trial-and-error experiments,^[8–10] and API inhomogeneity raises a potential risk that causes overdosed or ineffective treatment.^[11]


1. Introduction

Pharmaceutical formulation plays an important role in transforming a drug substance into the final drug product taken by a patient. It involves processes that combine an active pharmaceutical ingredient (API) and a mixture of inactive excipients into a final drug product with desired therapeutic effects and physical properties.^[1] Among various drug products, oral solid dosage forms are the most preferred product forms dominating the market because of their high patient compliance and wide

Methylcellulose (MC) and hydroxypropyl methylcellulose (HPMC) are two types of natural-based cellulose ester excipients that have been widely formulated into oral solid dosage forms in food and pharmaceutical applications.^[12–14] Their unique swelling and erosion behaviors are suitable for the design of controlled release systems and for the study of drug delivery models.^[15] Upon contact with water, a gel layer can form on the polymer surface due to rapid hydration, which slows down further water penetration into the inner dry polymer core.^[16] In addition, fast release can be easily achieved with the use of MC which shows a much faster matrix erosion than HPMC.^[14] Despite these ideal properties, formulations of these cellulose esters and hydrophobic APIs into drug products still lack efficient control over API nanocrystal sizes and heavily depend on multiple blending, sieving, and granulation steps.^[17,18] Reversible thermal gelation is another “smart” property of MC and HPMC that has gained considerable attention in the field of rheology^[19,20] and tissue engineering.^[21,22] The polymer gels upon heating and returns back to the sol state upon subsequent cooling.^[20] Although researchers have applied this property to develop in situ gelling materials for drug delivery,^[23,24] the utility of the thermal gelation property

L.-H. Chen, Prof. P. S. Doyle
Department of Chemical Engineering
Massachusetts Institute of Technology
77 Massachusetts Avenue, Cambridge, MA 02139, USA
E-mail: pdoyle@mit.edu

Prof. P. S. Doyle
Campus for Research Excellence and Technological Enterprise
Singapore 138602, Singapore

 The ORCID identification number(s) for the author(s) of this article can be found under <https://doi.org/10.1002/adma.202008618>.

DOI: 10.1002/adma.202008618

in the formulation of oral solid dosage forms still remains unexplored.

In recent years, hydrogels have been exploited as promising materials for drug product formulations because they can be readily customized into particles with various sizes and shapes.^[25–27] However, hydrogels are hydrophilic in nature and incompatible with hydrophobic drugs.^[28,29] To address the incompatibility issue and induce API nanocrystallization in the hydrogel matrix, novel technologies have been developed by incorporating hydrophobic nanodomains into hydrophilic hydrogels.^[30–34] The hydrophobic nanodomains, such as oil-in-water nanoemulsions and surfactant micelles, are able to control the formation of API nanocrystals in the hydrogel matrix with tailored drug loading contents. However, hydrogel formation is greatly limited to materials with well-known gelation techniques, such as free radical photopolymerization^[34] and ionic-crosslinking.^[31–33] These materials are generally not the most ideal excipients for oral drug formulation due to their slow release,^[34] large release resistance at high drug loadings,^[30,32,33] and potential toxicity.^[35] MC is an attractive fast-eroding excipient without the above limitations, though formulation approaches have generally not taken advantage of its gelation properties in forming the drug product. To bridge the gap between the use of fast-eroding MC and the efficiency of oral drug formulation, we report a new thermogelling nanoemulsion system. We develop facile thermal processing methods for the preparation of composite particles and versatile dosage forms with hydrophobic API nanocrystals embedded in the MC matrix.

2. Results and Discussion

To synthesize the thermogelling nanoemulsion, we use MC as both an emulsifier and gelling agent because of its dual amphiphilic and thermoresponsive properties. Fenofibrate is chosen as a hydrophobic model API owing to its extremely low water solubility ($0.3 \mu\text{g mL}^{-1}$ at 37°C).^[36] Anisole is used as a solvent to dissolve fenofibrate because it is approved for pharmaceutical formulation and has a high solubility for hydrophobic APIs.^[33] The continuous water phase contains a 5 wt% MC and the dispersed oil phase is an anisole solution saturated with fenofibrate. By ultrasonication a mixture of the water and oil phases, oil nanodroplets are formed with the MC hydrophobic units adsorbing on the droplet surface. The gelling mechanism of the MC-stabilized nanoemulsion is proposed schematically in **Figure 1a**. At low temperatures, the nanodroplets are uniformly dispersed and the free MC chains are soluble in the water phase. As the temperature increases, the MC hydrophobic units associate strongly into hydrophobic junctions,^[37] forming a gel network with the oil nanodroplets locally immobilized in the gel matrix. The proposed mechanism is supported by the temperature ramp experiment with a gel point of 29°C (Figure S1a, Supporting Information). Moreover, nanoemulsions with different formulations (Table S1, Supporting Information) are prepared to explore the parameter space for tuning the nanoemulsion properties. Introducing additional Tween 80 surfactant results in a stronger emulsifying ability and thus the formation of smaller nanodroplets (Figure 1b). The addition of 0.1 g Tween 80 is found to effectively reduce the nanodroplet

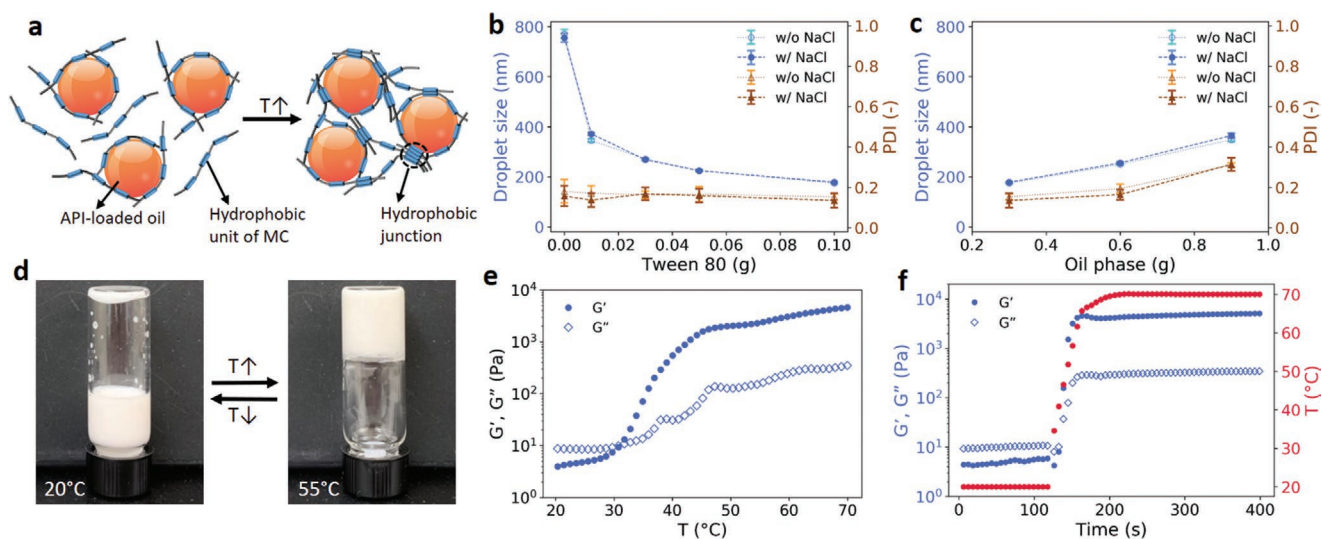


Figure 1. Overview of the nanoemulsion properties. a) Schematic diagram of the thermogelling mechanism. At low temperatures, the nanoemulsion suspension is composed of dispersed MC-stabilized oil nanodroplets and dissolved MC molecules. At elevated temperatures, the hydrophobic groups of MC associate together and a gel network is formed with the oil nanodroplets locally locked inside the thermogel matrix. b) Average droplet sizes (diameter) and polydispersity indexes (PDIs) for nanoemulsions with different Tween 80 mass (0, 0.01, 0.03, 0.05, 0.1 g) before and after 0.1 g NaCl addition. c) Average droplet sizes (diameter) and PDIs for nanoemulsions with different oil phase mass (0.3, 0.6, 0.9 g) before and after 0.1 g NaCl addition. d,e) Thermal gelation property of a representative nanoemulsion (3 g MC solution, 0.3 g oil phase, 0.05 g Tween 80, 0.1 g NaCl). d) Optical images of the nanoemulsion in an inverted glass vial at temperatures of 20 and 55 °C. e) Storage modulus (G') and loss modulus (G'') of the nanoemulsion in the temperature ramp experiment at a heating rate of 2°C min^{-1} (0.1% strain, 20 rad s^{-1} frequency). Apparent gel point is defined as the cross-over point between G' and G'' . f) Viscoelastic moduli of the nanoemulsion in the temperature jump experiment from a sol state (20°C) to a gel state (70°C) (0.1% strain, 20 rad s^{-1} frequency).

size to ≈ 175 nm and provide excess Tween 80 for increasing the oil phase in Figure 1c (Section S1, Supporting Information). Because the nanoemulsion is stabilized by the nonionic emulsifiers (MC and Tween 80), the incorporation of NaCl into the water phase does not perturb the kinetically stable nanoemulsion. The average droplet size and polydispersity index (PDI) remain almost identical after the NaCl addition (Figure 1b,c). The good stability of the nanoemulsion to NaCl provides another parameter for potential process improvement. Cl^- ions (salt-out ions) can compete with MC molecules for water hydration, which facilitates and strengthens hydrophobic association of MC into a gel network for better material encapsulation.^[38] To demonstrate the thermal gelation property, a representative nanoemulsion (3 g MC solution, 0.3 g oil phase, 0.05 g Tween 80, 0.1 g NaCl) is characterized with the results shown in Figure 1d–f. The liquid nanoemulsion gels and becomes solid-like in an inverted glass vial at an elevated temperature (Figure 1d). The apparent gel temperature is determined to be ≈ 31 °C in the temperature ramp experiment (Figure 1e). The effects of each nanoemulsion component on the gel temperature are discussed in Section S2 (Supporting Information), where gel points below 35 °C are reported for different nanoemulsion formulations. Furthermore, the nanoemulsion gels quickly in response to an abrupt temperature jump (Figure 1f). The combination of the low gel point and fast thermorespon-

sive nature of the nanoemulsion enables the formation of nanoemulsion thermogel with simple thermal processing.

Using the thermal gelation property of the nanoemulsion, a facile process is developed to formulate the nanoemulsion into thermogel particles by dripping the nanoemulsion into a heated water bath. The liquid nanoemulsion gels into thermogel particles in response to the sudden temperature change when contacting the water bath (Figure 2a). To prepare spherical particles by dripping a gelling material into a miscible gelation bath, the gelling material has to be sufficiently viscous to overcome the impact and drag forces exerted by the surrounding water.^[39] Without any additional thickening agent, the nanoemulsion system can easily achieve a high viscosity by decreasing the droplet size and increasing the oil fraction (Figure S2a, Supporting Information). With the addition of 0.05 g Tween 80, the nanoemulsion has a viscosity that facilitates the formation of spherical thermogel particles (Section S3, Supporting Information). In this work, we choose 0.1 g surfactant and 0.3 g oil phase (with fixed 5 g MC solution and 0.1 g NaCl) as the canonical condition. Figure 2b shows the thermogel particles prepared with an 18-gauge dispensing tip using the canonical condition. The particles are nearly spherical with a diameter of 2.72 ± 0.12 mm. Solving for the transient heat transfer in the droplet (Section S4, Supporting Information), the droplet surface quickly gels in 10 ms, and the droplet defined by the gelled

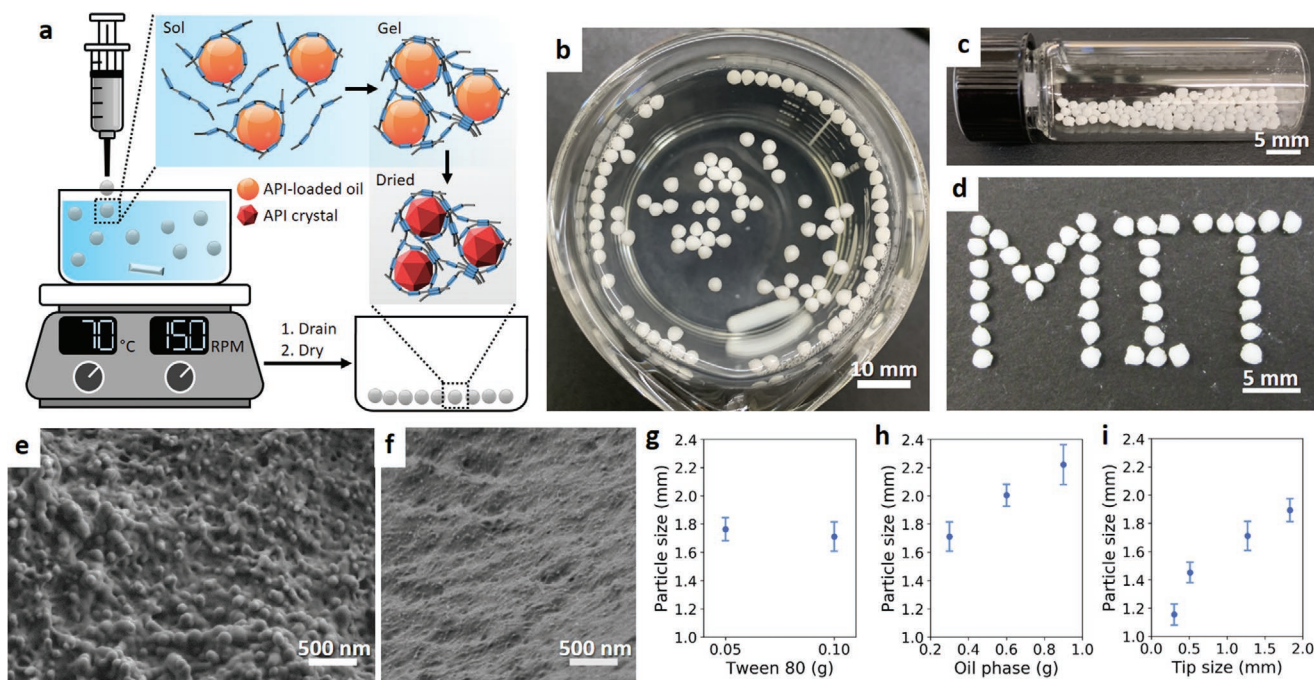


Figure 2. Overview of the particle formulation using the thermal dripping process. a) Schematic diagram of the thermal dripping process. A nanoemulsion at room temperature (≈ 20 °C) is dripped into a 70 °C water bath stirred at 150 rpm. Once the dripped droplet enters the water bath, the nanoemulsion gels rapidly in response to the temperature jump. After water removal and solvent evaporation, API nanocrystals are induced locally within the nanodroplets locked within the thermogel network. b–e) Particle formation with the canonical nanoemulsion (3 g MC solution, 0.3 g oil phase, 0.1 g Tween 80, 0.1 g NaCl). b) Optical image of thermogel particles formed by dripping the nanoemulsion into a 70 °C water bath with an 18-gauge dispensing tip. The hydrated particle diameter is 2.72 ± 0.12 mm. c,d) Optical image of dried particles in a glass vial and on a flat surface, respectively. The dried particle diameter is 1.71 ± 0.10 mm. e) SEM image of the embedded nanocrystals in the dried particles. f) SEM image of the internal structure of the dried MC particles without drug. g–i) Correlations between the particle size and various parameters: g) Tween 80 mass (with an 18-gauge dispensing tip), h) oil phase mass (with an 18-gauge dispensing tip), and i) dispensing tip outer diameter (with the canonical formulation). Scale bars for (b), (c,d), and (e,f) are 10, 5, and 500 nm, respectively.

surface can completely gel in 1.5 s (Figure S3, Supporting Information). Fast gelation leads to effective encapsulation with no nanoemulsion leakage detectable by dynamic light scattering. In addition, fenofibrate diffusion from the oil phase to the surrounding water bath is minimal because of the stark difference in fenofibrate solubility. The drug loading efficiencies for all formulations are greater than 99.4 wt%, indicating nearly perfect drug encapsulation (Section S5, Supporting Information). The bath water volume is adjusted until the water film thickness is comparable to the particle size, and then the gelation container is directly dried in a 70 °C oven without any additional washing step. During the drying, the oil nanodroplets are immobilized in the MC network and define individual crystallization domains, locally inducing API nanocrystals embedded in the dried MC matrix (Figure 2a). The dried thermogel particles (canonical condition) have a particle size of 1.71 ± 0.10 mm (Figure 2c,d), corresponding to 75% volume shrinkage of the hydrated particles. The importance of NaCl addition is demonstrated in a control experiment in which the resulting dried particles without NaCl addition buckle owing to weak MC hydrophobic association (Figure S6, Supporting Information). To observe the confined crystallization enabled by the nanoemulsion templating, scanning electron microscopy (SEM) imaging is performed on dried API-loaded particles (Figure 2e) and pristine MC particles without drug (Figure 2f). Compared to the pristine MC matrix, the API-loaded particles show clear evidence of embedded nanocrystals in the matrix. The observed nanocrystals have a diameter of 120.6 ± 13.6 nm, which is similar to the predicted nanocrystal diameter (≈ 131.7 nm) based on the oil nanodroplet size and API properties (Section S7, Supporting

Information). For different nanoemulsion formulations, the observed nanoparticle size in the MC matrix follows the estimated nanocrystal size (Figure S7f, Supporting Information), providing evidence of confined crystallization in the nanodroplets. The sizes of the dried particles are also investigated for different formulations (Figure 2g–i). With the same dispensing tip size, the particle size increases with increasing oil phase mass because a higher oil fraction can create a higher solid content after drying (Figure 2h). With the same nanoemulsion formulation, the particle size can be effectively controlled by varying the dispensing tip diameter (Figure 2i), and the correlation can be well described by the Tate's law (Figure S8g, Supporting Information).

Strategies to increase API loading in a drug product are important because of the great interest to develop smaller drug products for better patient compliance. However, iterative optimization of multiple processing steps are generally required for oral drug formulations with high drug loading contents.^[40] Figure 3a shows the drug loading contents of the dried API-loaded particles as a function of the oil phase mass. The measured drug loading contents lie between the theoretically maximal (blue dashed curve) and minimal (green dashed-dotted curve) values, and the loading content curve with 100% and 30% retention for Tween 80 and NaCl (orange dotted curve) is found to well describe the measured drug loading contents (Section S9, Supporting Information). With the nanoemulsion system, the drug loading content can be easily scaled up by adding more oil phase without any optimization required of the formulation and process. X-ray diffraction (XRD), Raman spectroscopy, and differential scanning calorimetry (DSC) are

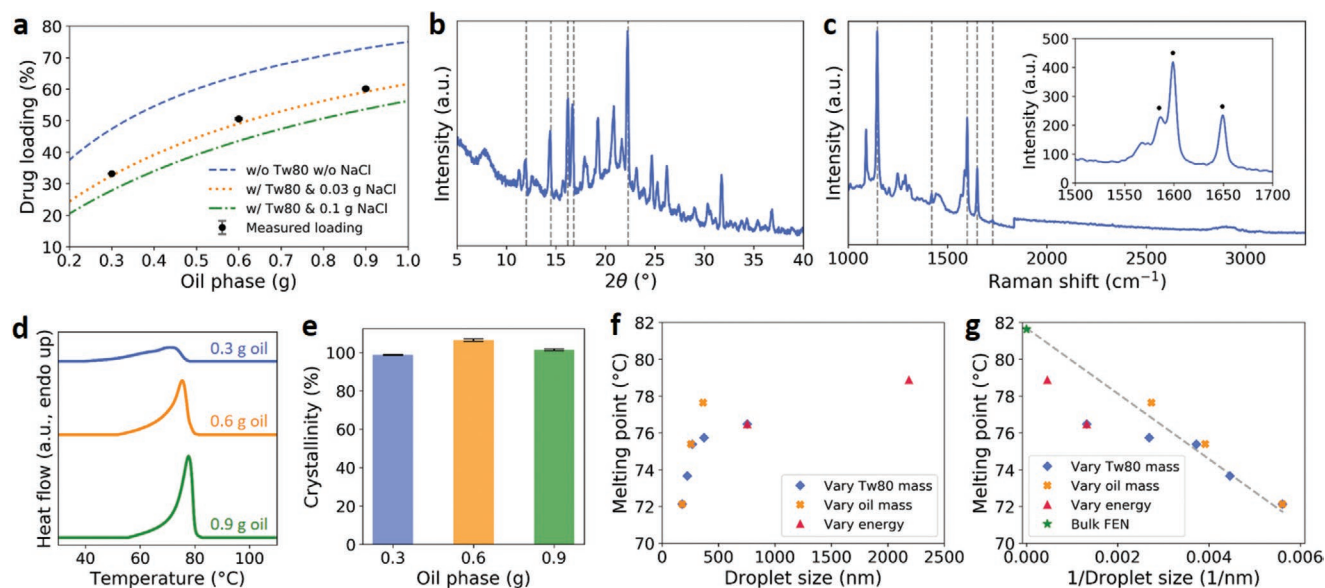


Figure 3. Characterization of the fenofibrate nanocrystals in the dried API-loaded particles. a) Drug loading content of the particles as a function of oil phase mass (fixed 3 g MC solution, 0.1 g Tween 80, 0.1 g NaCl). The blue dashed curve corresponds to Equation (5) with $\zeta_{\text{Tw80}} = 0$ and $\zeta_{\text{NaCl}} = 0$ (complete removal of Tween 80 and NaCl). The orange dotted curve corresponds to Equation (5) with $\zeta_{\text{Tw80}} = 1$ and $\zeta_{\text{NaCl}} = 0.3$ (100% and 30% retention for Tween 80 and NaCl). The green dashed-dotted curve corresponds to Equation (5) with $\zeta_{\text{Tw80}} = 1$ and $\zeta_{\text{NaCl}} = 1$ (complete retention of Tween 80 and NaCl). b) X-ray pattern and c) Raman spectrum of the fenofibrate nanocrystals in the particles. The inset is the zoomed-in high-frequency Raman spectrum. The dashed lines and black dots indicate the characteristic peaks for crystalline form I fenofibrate. d) DSC thermograms and e) crystallinity of the fenofibrate nanocrystals in the particles for different oil phase mass. f) Correlation between the melting point and droplet size. g) Correlation between the melting point and the reciprocal of droplet size. The bulk fenofibrate is assumed to be templated by an infinitely large droplet ($1/\text{droplet size} \approx 0$).

used to characterize the polymorphism and crystallinity of the fenofibrate nanocrystals in the particles. The XRD pattern in Figure 3b confirms the existence of fenofibrate nanocrystals in the particles, with the characteristic peaks aligning with those of crystalline form I fenofibrate at the diffraction angles (2θ) of 12° , 14.5° , 16.2° , 16.8° , and 22.4° .^[41] Form I fenofibrate is a desirable form because of its thermodynamic stability compared to the metastable form II and amorphous counterparts. The Raman spectrum also supports that the fenofibrate nanocrystals are form I polymorph (Figure 3c and Figure S11b, Supporting Information).^[41,42] DSC analyses not only suggest the presence of fenofibrate nanocrystals with a single endothermic peak of melting (Figure 3d) but also show a high degree of crystallinity ($\approx 100\%$ in Figure 3e) approximated with the prior knowledge of decreasing fusion enthalpy for lower melting points^[34,43] (Section S11, Supporting Information). The Gibbs–Thomson equation predicts that melting point depression becomes more significant for smaller nanocrystals. Compared to the as-received bulk fenofibrate crystals with a melting point of 81.7°C (Figure S11c, Supporting Information), the nanocrystal melting point decreases with decreasing nanoemulsion droplet size (Figure 3f). The melting point depression indicates the effectiveness of nanoemulsion droplets for templating API nanocrystals. Moreover, a linear trend is observed between the melting point and the reciprocal of the droplet size (Figure 3g). In a prior study, this linear trend was predicted and experimentally realized by carefully confining API crystallization in the nanopores of commercial pore glass.^[43] However, unlike the rigid templates that are limited to certain specifications, “soft” templates enabled by the nanoemulsion provide a flexible approach to simultaneously control the drug crystal size

and the drug loading content (i.e., crystal density) for designing a wide range of drug products.

Next, the release performance of the API-loaded dried particles was evaluated and compared to that of bulk fenofibrate crystals (Figure 4a and complete release profile in Figure S13a, Supporting Information). The bulk crystals with a size of $\approx 239.6\ \mu\text{m}$ (Figure S9a, Supporting Information) are nearly insoluble—it takes 12.1 h to reach 80% release and another 19.4 h to reach complete release. As expected, all the nanocrystal-loaded particles show a significantly faster release (Figure 4a,b and Figure S13b, Supporting Information). For different oil phase mass, the release profiles are nearly identical (Figure 4a), which is ideal for maintaining the release performance when the drug loading content is increased. In Figure 4b, varying the particle size for the same nanoemulsion is shown to be an effective approach to engineer the release profile, with the reduction of particle size accelerating the drug release. Furthermore, the crushed particles with the similar size of the bulk fenofibrate crystals show a very fast drug release—5.4 min to reach 80% release and another 8.6 min to reach complete release (purple curve in Figure 4b). The fast release is attributed to the combination of the nanosized API crystals and faster-eroding MC matrix. Figure 4c shows the 80% release time (t_{80}) with respect to the drug loading content. The t_{80} can be easily tuned by varying the particle size with the same formulation (vertical change in Figure 4c) and is maintained nearly constant with increasing drug loading content (horizontal change in Figure 4c). The constant t_{80} over a wide range of drug loading content can facilitate the design of drug products with a good control over the release performance. Although we have previously shown that alginate hydrogels formulations have fast

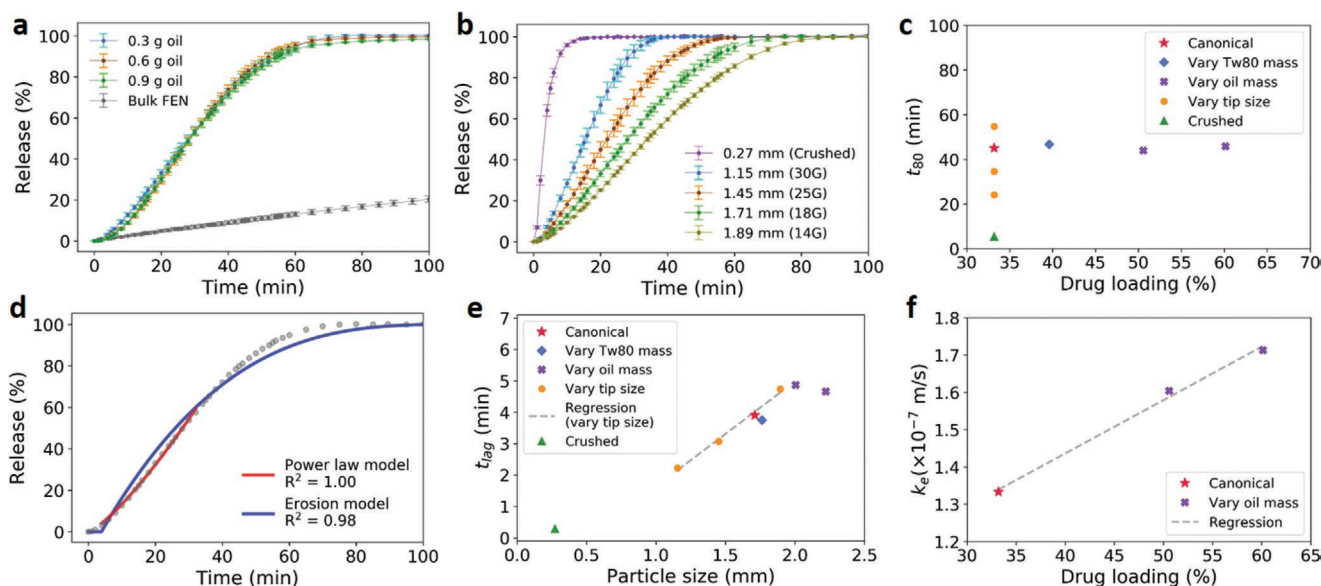


Figure 4. Release performance and analyses of the dried API-loaded particles. a) Cumulative release profiles of the as-received bulk fenofibrate crystals (diameter $\approx 239.6\ \mu\text{m}$) and the particles with different oil phase addition (fixed 3 g MC solution, 0.1 g Tween 80, 0.1 g NaCl). b) Cumulative release profiles of particles with different diameters (obtained via crushing and varying dispensing tip size for the canonical formulation). The legend includes the particle diameter and tip specification. c) Time at 80% drug release (t_{80}) plotted versus the drug loading content for different conditions. d) Fitting the release profile of the canonical condition with the power law and erosion models. e) Correlation between the lag time (t_{lag}) and particle size. f) Correlation between the erosion constant (k_e) and drug loading content.

release that performs very well against the commercial fenofibrate product, the release rate plummets as the drug loading content exceeds 40% (Figure S13g, Supporting Information).^[32] The release mechanism of alginate hydrogels is through dissolution and diffusion,^[31] and above a certain drug loading content threshold the dissolved drug molecules cannot diffuse out effectively for further dissolution. In contrast, the MC particles not only show an even faster release than alginate particles at lower loading contents but also maintain the good performance at high loading contents using both the erosion rate (a/t_{80}) and diffusivity (a^2/t_{80}) metrics (Figure S13h,i, Supporting Information). To understand the release mechanism of the particles with the MC matrix, a power law model (Figure 4d with Equation (S26), Supporting Information) is used to fit the release profiles.^[44] The exponent n values are greater than 1.2 for all cases (Figure S14a, Supporting Information), indicating the drug release is strongly erosion-controlled.^[45] This finding agrees well with the observation that the drug release occurs with the eroding matrix and is complete once the particles are fully eroded. The synchronous behavior of the drug release and particle erosion implies that nanocrystals dissolve very fast and the drug dissolution is no longer a rate-determining step. To further analyze the release kinetics, an erosion model for an erodible sphere (Figure 4d with Equation (S32), Supporting Information) is used to determine the erosion constant and lag time.^[46] The lag time is introduced to account for the release suppression owing to the initial wetting of the dried particles when they first contact water.^[47] The lag time is positively correlated with the particle size (Figure 4e). The smaller particles have a larger surface area for faster hydration before the erosion plays an important role. For the crushed particles, the wetting and erosion almost happen simultaneously with the lag time approaching zero. Moreover, the erosion model accounting for the particle size can help explain the convoluted effects on the release profiles. Increasing the oil phase mass corresponds to a larger ratio of the dispersed to continuous phases, and the resulting dried particles have a higher drug loading content and a lower MC polymer content. Therefore, although the particles are larger for more oil phase addition (Figure 2h), the lower polymer content leads to a faster erosion rate (Figure 4f). The two factors offset each other and maintain a nearly constant performance when the oil phase is increased (Figure 4a).

In addition to the aforementioned particle formulation, the thermogelling nanoemulsion with “smart” responsiveness to temperature can be easily crafted into versatile dosage forms by simple thermal treatment. For the preparation of nanoparticle suspensions, conventional processes are typically time-consuming and can take more than 10 h to mill down API crystals to a desirable nanoscale range.^[48] In contrast, soft oil droplets can be easily broken up into nanodroplets in five minutes and approach the minimum droplet size in 20 min.^[49] Ethyl acetate is chosen as a fast-evaporating solvent (boiling point of 77.1 °C) to load fenofibrate to induce API nanocrystals before the water phase has dried out. With the same water phase (3 g 5 wt% MC) and 0.1 g Tween 80, the oil phase of a 0.1 g-fenofibrate-in-0.3 g-ethyl-acetate solution is used to form a thermogelling nanoemulsion (Figure 5a). Gelled at 50 °C, the nanoemulsion is then evaporated at the same temperature (Figure 5b) until twice the mass of the added ethyl acetate (≈ 0.6 g) is removed to

ensure the complete removal of ethyl acetate. The still hydrated thermogel is redispersed into deionized water to form a polymer-stabilized nanoparticle suspension, and the uniform nanoparticles cannot be only detected by dynamic light scattering but also observed by transmission electron microscopy (TEM) (Figure 5c). The nanoparticles (≈ 216.7 nm) are found to be larger than the nanoemulsion droplets (≈ 129.5 nm), suggesting that more MC molecules adsorb on the nanocrystals for better stability after redispersion (Figure S15, Supporting Information). To demonstrate the utility of the thermogel in producing nanocrystals, a control evaporation test conducted at room temperature (below the gel point) shows undesirable nanoemulsion destabilization (Figure 5d) and large crystal precipitation (Figure 5e). Moreover, a thermal molding method is developed to prepare drug tablets (Figure 5f,g). Instead of relying on the multistep mixing/transport of API crystals and excipient powders as in the conventional manufacturing,^[17,18] drug tablets with embedded API nanocrystals can be directly formulated in a facile and powderless manner. Without the issue about stimulus penetrability,^[50] heat flux from the environment can easily penetrate through the nanoemulsion in the mold and ensure the complete gelation. The gelled nanoemulsion is then evaporated in situ for 1 d and the drug tablets are formed (Figure 5g). Finally, the nanoemulsion can be thermally cast into oral thin films, which are novel dosage forms that have gained considerable attention in recent years because of their exceptional acceptability for geriatric and pediatric patients.^[51] The use of the thermogelling nanoemulsion can avoid dealing with drug crystal agglomeration that is still a common problem in the conventional casting process.^[52] By gelling and evaporating a liquid film of the nanoemulsion on a poly(dimethylsiloxane) (PDMS) substrate (Figure 5h–j), a paper-like oral thin film with a thickness of ≈ 20 μm can be easily prepared (Figure 5k).

3. Conclusion

We have developed a new thermogelling nanoemulsion system that can be easily formulated into composite solid dosage drug products with well-controlled API nanocrystals embedded in the MC matrix. The nanoemulsion suspension has a low gel temperature and fast response to temperature changes which enable the realization of effective particle formulation with a thermal dripping method. The thermally gelled nanoemulsion can be directly dried with the precise formation of API nanocrystals templated by the nanodroplets. The API nanocrystals are characterized to be the most stable polymorph and their presence is validated by SEM, XRD, Raman spectroscopy, and DSC analyses. The significantly improved dissolution rate of the nanocrystals is demonstrated in release tests. The fast drug release is not limited by the dissolution of the API nanocrystals and directly controlled by the fast erosion of the MC matrix. Moreover, the release can be easily tuned by varying the particle size, and fast release is maintained for a wide range of drug loading contents. To demonstrate the versatility of the nanoemulsion formulation, various dosage forms (nanoparticle suspension, drug tablet, and oral thin film) are prepared with a simple and efficient thermal treatment. Overall, the thermogelling nanoemulsion holds significant potential for more efficient

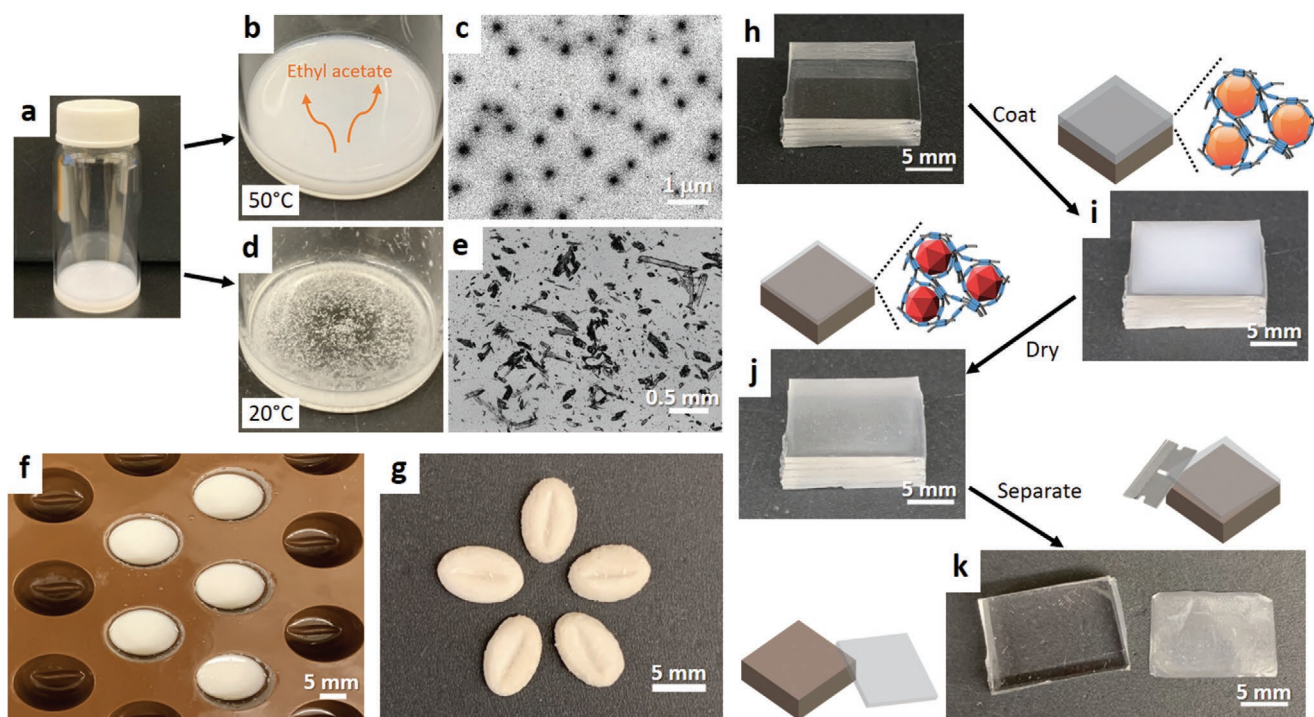


Figure 5. Versatility of the thermogelling nanoemulsion in pharmaceutical formulations for various dosage forms. a) Optical image of the nanoemulsion with the oil phase of a fenofibrate-in-ethyl-acetate solution (0.1 g fenofibrate, 0.3 g ethyl acetate). The resulting nanoemulsion has a diameter d_{drop} of 129.5 nm and PDI of 0.195. b) Optical image of the nanoemulsion thermogel after ethyl acetate is evaporated at 50 °C. The redispersed nanoparticle suspension has a diameter of 216.7 nm and PDI of 0.218 (measured by dynamic light scattering). c) TEM image of the redispersed nanoparticle suspension (diameter 201.4 ± 34.2 nm). d) Optical image of the nanoemulsion after ethyl acetate is evaporated at room temperature in a circulating fume hood (≈ 20 °C). Large fenofibrate crystals precipitate out as droplets are not held in place via a gel network. e) Bright-field microscopy image of the large crystals from (d). f) Optical image of a coffee-bean mold loaded with the thermogelling nanoemulsion (0.5 mL in one slot). g) Optical image of the drug tablets in a coffee-bean shape after solvent evaporation of the thermogel at 70 °C. h–k) Formulation of oral thin films. h) Pristine PDMS acts as a platform for thin-film casting. i) The platform is applied with a nanoemulsion thin film of 0.1 mL. j) The thin film is gelled and dried at 55 °C on the platform. k) Separated from the platform, an oral thin film with a thickness of ≈ 20 μm is formed. Scale bars for (c), (e), and (f–k) are 1 μm , 0.5 mm, and 5 mm, respectively.

formulation of oral drug products with high quality and tunable fast release.

4. Experimental Section

Materials: Methylcellulose (viscosity: 15 cP, molecular weight $\approx 14\,000$ g mol⁻¹), Tween 80 (polysorbate), fenofibrate, anisole, ethyl acetate, sodium chloride (NaCl), ethanol, and sodium dodecyl sulfate (SDS) were purchased from Sigma-Aldrich and used without further purification steps.

Synthesis of Thermogelling Nanoemulsions: Prior to nanoemulsion synthesis, the continuous water and dispersed oil phase solutions were first prepared. The continuous water phase was a 5 wt% methylcellulose aqueous solution. The dispersed oil phase was a saturated fenofibrate-in-anisole solution, which was prepared by adding fenofibrate into anisole until excessive fenofibrate crystals settled down in the bottle and could not be further dissolved. To prepare the nanoemulsion, a preemulsion was first prepared by vortexing a mixture of the continuous phase, dispersed phase, and Tween 80 in a 50 mL Falcon conical centrifuge tube. The preemulsion was then ultrasonicated at 30% amplitude in an ultrasonicator with a 24 mm diameter horn (from Cole Parmer) at a frequency of 20 kHz for 30 min. The ultrasonicator was kept at 10 °C using a cooling circulating water bath. The as-prepared ion-free nanoemulsion was added with 0.1 g NaCl and vortexed for another 30 s.

The parameter space for the nanoemulsion synthesis is summarized in Table S1 (Supporting Information). The droplet size and PDI of the nanoemulsion were measured by dynamic light scattering (Brookhaven NanoBrook 90Plus PALS) operated at a fixed scattering angle of 90° and a temperature of 25 °C. The sample was prepared by diluting ≈ 5 μL of the nanoemulsion solution with 3 mL deionized water in a cuvette. For each sample, five sets of 1-min measurements were done to determine the droplet size distribution.

Rheological Characterization of Nanoemulsions: Rheological properties of nanoemulsions were characterized using a stress-controlled rheometer (DHR-3, TA instrument) equipped with an upper-cone geometry (diameter = 60 mm, cone angle = 1.004°, and truncated gap = 29 μm) and a temperature-controlled Peltier lower-plate. To minimize the evaporation, a few water drops were added on top of the cone geometry and a solvent trap was used. Before each measurement, a conditioning procedure was performed at 20 °C: a preshear at a constant rotational speed of 10 rad s⁻¹ for 60 s, followed by an equilibration duration of 60 s. Temperature ramp measurements were conducted from 20 to 70 °C with a heating rate of 2 °C min⁻¹, a strain amplitude of 0.1%, and frequency of 20 rad s⁻¹. Temperature jump experiments were performed from 20 to 70 °C with a strain amplitude of 0.1% and a frequency of 20 rad s⁻¹. Viscosities were measured with the shear rate sweeping from 1 to 1000 s⁻¹ at 20 °C.

Preparation of Thermogel Particles: Thermogel particles were prepared by a thermal dripping method. The gelation bath was a 300 mL 70 °C deionized water added with 0.1% w/v Tween 80 to lower the surface

tension. 2–3 mL of the thermogelling nanoemulsion was loaded into a 3 mL syringe and dripped into the bath at a dripping height of 1 cm. The stirring rate was maintained at 150 rpm to enhance the heat transfer. Different dispensing tips were used to vary the particle size: smooth-flow tapered tips (14, 18, and 25 gauge) and precision stainless steel tip (30 gauge). After the dripping, the water was removed from the gelation bath until the height of the remaining water was comparable to the particle size. The gelation container carrying the particles and water thin film was quickly transferred to a 70 °C oven and dried for 1 d to evaporate anisole and water. The dried thermogel particles were stored at room temperature before characterization and release tests.

Estimation of Drug Loading Efficiency and Drug Loading Content: Drug loading efficiency (L_E) is estimated as follows

$$m_{\text{opt}} = m_{\text{NE}} \Psi_{\text{FEN/NE}} \quad (1)$$

$$\Psi_{\text{FEN/NE}} = \frac{m_o \omega_{\text{FEN}}}{m_c + m_o + m_{\text{Tw80}} + m_{\text{NaCl}}} \quad (2)$$

$$m_{\text{bath}} = C_{\text{bath}} V_{\text{bath}} \quad (3)$$

$$L_E = 1 - \frac{m_{\text{bath}}}{m_{\text{opt}}} \quad (4)$$

where m_{opt} is the optimal fenofibrate mass carried by the as-prepared nanoemulsion, m_{NE} is the mass of nanoemulsion dripped into the heated water bath (with 0.1% w/v Tween 80), $\Psi_{\text{FEN/NE}}$ is the fenofibrate weight fraction in the as-prepared nanoemulsion, m_o is the oil phase mass, ω_{FEN} is the fenofibrate weight fraction in the oil phase ($\approx 45 \text{ wt}\%$ ^[32]), m_c is the mass of the continuous water phase, m_{Tw80} is the Tween 80 mass, m_{NaCl} is the NaCl mass, m_{bath} is the mass of fenofibrate diffusing into the bath, C_{bath} is the fenofibrate concentration in the bath after the dripping process, and V_{bath} is the bath volume.

Drug loading content (ϕ_{FEN}) is estimated by

$$\phi_{\text{FEN}} = \frac{m_o \omega_{\text{FEN}}}{m_c \omega_{\text{MC}} + m_o \omega_{\text{FEN}} + \zeta_{\text{Tw80}} m_{\text{Tw80}} + \zeta_{\text{NaCl}} m_{\text{NaCl}}} \quad (5)$$

where ω_{MC} is the MC weight fraction in the water phase (5 wt%), ζ_{Tw80} is the retention rate of Tween 80 in the dried particles, and ζ_{NaCl} is the retention rate of NaCl in the dried particles.

Drug Loading Content Measurement: The drug loading content of the dried particles was determined by a UV–vis spectrophotometer (Thermo Scientific NanoDrop One). A concentration–absorbance calibration curve was first established using fenofibrate-in-ethanol solutions with different concentrations ranging from 0.01 to 0.5 mg mL⁻¹. From the UV–vis absorbance spectra recorded from 150 to 850 nm, the absorbance peak values occurring at 287 nm (due to carbonyl groups of fenofibrate) were used for developing the calibration curve. For determination of drug loading content, dried particles were first cut into fine powders using a razor blade. Then, 10 mg fine powders were added with 3 mL ethanol, and the mixture was vortexed for 1 min. After the powders settled down by gravity, the ethanol solution was sampled and diluted ten times for UV–vis measurements. All measurements were done in triplicate.

XRD Analysis: The crystalline structures of the as-received bulk fenofibrate crystals and the fenofibrate nanocrystals in the dried particles were characterized by XRD using an in-reflection mode (Philips PANalytical X'Pert Pro MPD). The samples were ground and placed on a silicon crystal zero diffraction plate. The instrument was operated at 40 kV with an anode current of 40 mA with the X-ray source generated using a copper anode (K α emission wavelength of 1.54 Å). The diffraction angle 2θ was swept from 4° to 40° with a step size of 0.01671° at a scanning rate of 2° min⁻¹.

DSC Analysis: The melting points of the as-received bulk fenofibrate crystals and the fenofibrate nanocrystals in the dried particles were determined using a differential scanning calorimeter (TA Instruments Q2000). Inert environment was maintained in the sample chamber using a nitrogen gas flow at 50 mL min⁻¹. For each measurement, Tzero

pans and lids were used with ≈ 5 mg of ground sample. A temperature ramp was performed from –10 to 150 °C at a heating rate of 10 °C min⁻¹.

Scanning Electron Microscopy: The fenofibrate nanocrystals in the dried particles were observed with high-resolution scanning electron microscope (Zeiss HRSEM) at 1 kV accelerating voltage and at a magnification of 30 000 \times . All samples were prepared on SEM specimen stubs with carbon tape. The SEM images were analyzed with ImageJ to estimate the nanocrystal sizes.

Drug Release Experiment: The in vitro release of the dried particles was measured using a USP Dissolution Apparatus II (Agilent Technologies Varian VK 7025). A Cary 50 UV–vis spectrometer and an in situ probe set, which were integrated in the dissolution apparatus, automatically recorded the absorbance at a wavelength of 287 nm every minute. The release medium was a 900 mL 25 $\times 10^{-3}$ M SDS aqueous solution. The operating temperature and paddle rotational speed were set at 37 °C and 75 rpm, respectively. For each dissolution test, the sample mass was adjusted based on its drug loading content to maintain the final fenofibrate concentration constant at 10 $\mu\text{g mL}^{-1}$. The release experiment for each sample was done in triplicate.

Preparation of Nanoparticle Suspensions: A dispersed oil phase of 0.1 g fenofibrate in 0.3 g ethyl acetate was first prepared and added with 3 g 5 wt% MC solution and 0.1 g Tween 80 for preparing the nanoemulsion. After the nanoemulsion was gelled at 50 °C in a capped vial for 5 min, the vial was uncapped to evaporate ethyl acetate until twice the mass of the added ethyl acetate (≈ 0.6 g) was removed. The still hydrated thermogel was then redispersed into deionized water to form an MC-stabilized nanoparticle suspension. Observations of the nanoparticles were carried out using an FEI Tecnai G2 Spirit TWIN TEM equipped with a LaB6 filament, operating at an accelerating voltage of 120 kV. The nanoparticle suspensions were drop-cast onto carbon film supported copper grids (size 200 mesh), and bright-field microscopy images were taken using a Gatan CCD camera.

Preparation of Drug-Loaded Tablets: A coffee-bean silicone mold was first applied with a small amount of cooking oil to prevent sticking. Each slot of the mold was filled with 0.5 mL of the nanoemulsion. Then, the nanoemulsion was gelled and evaporated in the mold at 70 °C for 1 d and drug-loaded tablets were formed.

Preparation of Oral Thin Films: A PDMS fragment (length \times width: 1.5 cm \times 1 cm) was used as a substrate for thin-film casting. 0.1 mL of the nanoemulsion was used to coat the PDMS top surface. Then, the PDMS substrate carrying the nanoemulsion thin film was transferred to a 55 °C air circulating oven with the nanoemulsion gelled and evaporated for 1 d. After separated from the substrate, an oral thin film was obtained.

Supporting Information

Supporting Information is available from the Wiley Online Library or from the author.

Acknowledgements

This research was supported in part by the NSF grant CMMI-1824297 and the Singapore National Research Foundation, Prime Minister's Office, Singapore under its Campus for Research Excellence and Technological Enterprise Program (CREATE). L.-H.C. was partially supported by a scholarship from Think Global Education Trust (Taiwan).

Conflict of Interest

Massachusetts Institute of Technology (MIT) has filed a provisional patent application on behalf of P.S.D. and L.-H.C. based on the research in this study.

Data Availability Statement

The data that support the findings of this study are available from the corresponding author upon reasonable request.

Keywords

hydrogel particles, hydrophobic drugs, nanocrystals, oral dosage forms, thermoresponsive nanoemulsions

Received: December 21, 2020

Revised: March 30, 2021

Published online:

- [1] D. Reker, S. M. Blum, C. Steiger, K. E. Anger, J. M. Sommer, J. Fanikos, G. Traverso, *Sci. Transl. Med.* **2019**, *11*, eaau6753.
- [2] H. Rosen, T. Aribat, *Nat. Rev. Drug Discovery* **2005**, *4*, 381.
- [3] S. V. Sastry, J. R. Nyshadham, J. A. Fix, *Pharm. Sci. Technol. Today* **2000**, *3*, 138.
- [4] T. Loftsson, M. E. Brewster, *J. Pharm. Pharmacol.* **2010**, *62*, 1607.
- [5] L. Gao, G. Liu, J. Ma, X. Wang, L. Zhou, X. Li, *J. Controlled Release* **2012**, *160*, 418.
- [6] J. U. A. H. Junghanns, R. H. Müller, *Int. J. Nanomed.* **2008**, *3*, 295.
- [7] B. E. Rabinow, *Nat. Rev. Drug Discovery* **2004**, *3*, 785.
- [8] A. Miwa, T. Yajima, S. Itai, *Int. J. Pharm.* **2000**, *195*, 81.
- [9] N. Willecke, A. Szepes, M. Wunderlich, J. P. Remon, C. Vervaet, T. De Beer, *Int. J. Pharm.* **2017**, *522*, 234.
- [10] N. Willecke, A. Szepes, M. Wunderlich, J. P. Remon, C. Vervaet, T. De Beer, *Int. J. Pharm.* **2018**, *545*, 128.
- [11] S. Oka, D. Smrčka, A. Kataria, H. Emady, F. Muzzio, F. Štěpánek, R. Ramachandran, *Int. J. Pharm.* **2017**, *528*, 578.
- [12] A. R. Patel, *Adv. Funct. Mater.* **2020**, *30*, 1806809.
- [13] Y. Cao, R. Mezzenga, *Nat. Food* **2020**, *1*, 106.
- [14] T. Dow, *Midland, MI Dow Chem. Co.* **2000**.
- [15] J. Siepman, N. A. Peppas, *Adv. Drug Delivery Rev.* **2012**, *64*, 163.
- [16] R. T. C. Ju, P. R. Nixon, M. V. Patel, *J. Pharm. Sci.* **1995**, *84*, 1455.
- [17] S. Kiortsis, K. Kachrimanis, T. Broussali, S. Malamataris, *Eur. J. Pharm. Biopharm.* **2005**, *59*, 73.
- [18] T. Ishikawa, Y. Watanabe, K. Takayama, H. Endo, M. Matsumoto, *Int. J. Pharm.* **2000**, *202*, 173.
- [19] K. Kobayashi, C. I. Huang, T. P. Lodge, *Macromolecules* **1999**, *32*, 7070.
- [20] N. Sarkar, *J. Appl. Polym. Sci.* **1979**, *24*, 1073.
- [21] K. Vulic, M. S. Shoichet, *J. Am. Chem. Soc.* **2012**, *134*, 882.
- [22] M. C. Tate, D. A. Shear, S. W. Hoffman, D. G. Stein, M. C. LaPlaca, *Biomaterials* **2001**, *22*, 1113.
- [23] D. Gupta, C. H. Tator, M. S. Shoichet, *Biomaterials* **2006**, *27*, 2370.
- [24] M. K. Bain, M. Bhowmik, S. N. Ghosh, D. Chattopadhyay, *J. Appl. Polym. Sci.* **2009**, *113*, 1241.
- [25] H. Z. An, M. E. Helgeson, P. S. Doyle, *Adv. Mater.* **2012**, *24*, 3838.
- [26] L. H. Chen, L. C. Cheng, P. S. Doyle, *Adv. Sci.* **2020**, *7*, 2001677.
- [27] J. Li, D. J. Mooney, *Nat. Rev. Mater.* **2016**, *1*, 16071.
- [28] N. A. Peppas, J. Z. Hilt, A. Khademhosseini, R. Langer, *Adv. Mater.* **2006**, *18*, 1345.
- [29] T. R. Hoare, D. S. Kohane, *Polymer* **2008**, *49*, 1993.
- [30] A. Z. M. Badruddoza, P. D. Godfrin, A. S. Myerson, B. L. Trout, P. S. Doyle, *Adv. Healthcare Mater.* **2016**, *5*, 1960.
- [31] A. Z. M. Badruddoza, A. Gupta, A. S. Myerson, B. L. Trout, P. S. Doyle, *Adv. Ther.* **2018**, *1*, 1700020.
- [32] T. Domenech, P. S. Doyle, *Chem. Mater.* **2020**, *32*, 498.
- [33] H. B. Eral, M. O'Mahony, R. Shaw, B. L. Trout, A. S. Myerson, P. S. Doyle, *Chem. Mater.* **2014**, *26*, 6213.
- [34] P. D. Godfrin, H. Lee, J. H. Lee, P. S. Doyle, *Small* **2019**, *15*, 1803372.
- [35] H. J. Moon, M. Ku, Y. H. Roh, H. J. Lee, J. Yang, K. W. Bong, *Langmuir* **2020**, *36*, 2271.
- [36] M. Vogt, K. Kunath, J. B. Dressman, *Eur. J. Pharm. Biopharm.* **2008**, *68*, 283.
- [37] L. Li, P. M. Thangamathesvaran, C. Y. Yue, K. C. Tam, X. Hu, Y. C. Lam, *Langmuir* **2001**, *17*, 8062.
- [38] Y. Xu, L. Li, P. Zheng, Y. C. Lam, X. Hu, *Langmuir* **2004**, *20*, 6134.
- [39] E. S. Chan, B. B. Lee, P. Ravindra, D. Poncet, *J. Colloid Interface Sci.* **2009**, *338*, 63.
- [40] L. Cai, L. Farber, D. Zhang, F. Li, J. Farabaugh, *Int. J. Pharm.* **2013**, *441*, 790.
- [41] A. Heinz, K. C. Gordon, C. M. McGoverin, T. Rades, C. J. Strachan, *Eur. J. Pharm. Biopharm.* **2009**, *71*, 100.
- [42] Y. Ying, C. Beck, A. Wu, R. Dave, Z. Iqbal, *J. Raman Spectrosc.* **2017**, *48*, 750.
- [43] L. M. Dwyer, V. K. Michaelis, M. O'Mahony, R. G. Griffin, A. S. Myerson, *CrystEngComm* **2015**, *17*, 7922.
- [44] P. L. Ritger, N. A. Peppas, *J. Controlled Release* **1987**, *5*, 37.
- [45] J. L. Ford, K. Mitchell, P. Rowe, D. J. Armstrong, P. N. C. Elliott, C. Rostron, J. E. Hogan, *Int. J. Pharm.* **1991**, *71*, 95.
- [46] H. B. Hopfenberg, in *Controlled Release Polymeric Formulations*, ACS Symposium Series, Vol. 33 (Eds: D. R. Paul, F. W. Harris), American Chemical Society, Washington, DC, USA **1976**, pp. 26–32.
- [47] L. Zhang, J. Alfano, D. Race, R. N. Davé, *Eur. J. Pharm. Sci.* **2018**, *117*, 245.
- [48] D. A. Shah, S. B. Murdande, R. H. Dave, *J. Pharm. Sci.* **2016**, *105*, 10.
- [49] A. Gupta, H. B. Eral, T. A. Hatton, P. S. Doyle, *Soft Matter* **2016**, *12*, 1452.
- [50] S. K. Suh, K. W. Bong, T. A. Hatton, P. S. Doyle, *Langmuir* **2011**, *27*, 13813.
- [51] S. Karki, H. Kim, S. J. Na, D. Shin, K. Jo, J. Lee, *Asian J. Pharm. Sci.* **2016**, *11*, 559.
- [52] L. Sievens-Figueroa, A. Bhakay, J. I. Jerez-Rozo, N. Pandya, R. J. Romañach, B. Michniak-Kohn, Z. Iqbal, E. Bilgili, R. N. Davé, *Int. J. Pharm.* **2012**, *423*, 496.